Closure of the Mott gap and formation of a superthermal metal in the Fröhlich-type nonequilibrium polaron Bose-Einstein condensate in UO2+x

Conradson, S.; Durakiewicz, T.; Tayal, A.; Andersson, D.; Bagus, P.; Baldinozzi, G.; Bishop, A.; Boland, K.; Bradley, J.; Byler, D.; Clark, D.; Conradson, D.; Espinosa-Faller, F.; Gilbertson, S. M.; Kas, J.; Kozimor, S.; Kvashnina, K.; Lezama-Pacheco, J.; Martucci, M.; Nordlund, D.; Rehr, J.; Rodriguez, G.; Seidler, G.; Valdez, J.;

Originally published:

September 2017

Physical Review B 96(2017), 125114

DOI: https://doi.org/10.1103/PhysRevB.96.125114

Perma-Link to Publication Repository of HZDR:

https://www.hzdr.de/publications/Publ-23399

Closure of the Mott Gap and formation of a superthermal metal in the Fröhlich-type, non-equilibrium, polaron Bose-Einstein condensate of $UO_{2(+x)}$

Steven D. Conradson,[a]* David A. Andersson,[b] Kevin S. Boland,[b] Joseph A. Bradley,[b,c] Darrin D. Byler,[b] Tomasz Durakiewicz,[b†] Steven M. Gilbertson,[b] Stosh A. Kozimor,[b] Kristina O. Kvashnina,[d] Dennis Nordlund,[e] George Rodriguez,[b] Gerald T. Seidler,[c] Paul S. Bagus,[f] Sergei M. Butorin,[g] Dylan R. Conradson,[b] Francisco J. Espinosa-Faller,[h] Nancy J. Hess,[i] Joshua J. Kas,[c] Juan S. Lezama-Pacheco,[j] Philippe Martin,[k] Mary B. Martucci,[l] John J. Rehr,[c] James A. Valdez,[b] Alan R. Bishop,[b] Gianguido Baldinozzi,[m] David L. Clark,[b] Akhil Tayal[n]

Mixed valence O-doped UO_{2+x} and photoexcited UO_2 containing transitory U^{3+} and U^{5+} host a coherent polaronic quantum phase (CPQP) that exhibits the characteristics of a Fröhlich-type, non-equilibrium, phonon-coupled Bose-Einstein condensate whose stability and coherence are amplified by collective, anharmonic motions of atoms and charges. Complementary to the available, detailed, real space information from scattering and EXAFS, an outstanding question is the electronic structure. Mapping the Mott gap in UO_2, U_4O_9, and U_3O_7 with O XAS and NIXS and U M_5 RIXS shows that O-doping raises the peak of the U 5*f* states of the valence band by ~0.4 eV relative to a calculated value of 0.25 eV. However, it lowers the edge of the conduction band by 1.5 eV vs. the calculated 0.6 eV, a difference much larger than the experimental error. This 1.9 eV reduction in the gap width constitutes most of the 2-2.2 eV gap measured by optical absorption. In addition, the XAS spectra show a tail that will intersect the occupied U 5*f* states and give a continuous density-of-states that increases rapidly above its constricted intersection. Femtosecond-resolved photoemission measurements of UO_2 coincident with the excitation pulse with 4.7 eV excitation show the unoccupied 5*f* states of UO_2 and no hot electrons. 3.1 eV excitation, however, complements the O-doping results by giving a continuous population of electrons for several eV above the Fermi level. The CPQP in photoexcited UO_2 therefore fulfills the criteria prescribed for a non-equilibrium condensate. The electron distributions resulting from both excitations persist for 5-10 ps, indicating that they are the final state that therefore forms without passing through the initial continuous distribution of nonthermal electrons observed for other materials. Three exceptional findings are: 1) the direct formation of both of these long lived (>3-10 ps) excited states without the short lived nonthermal intermediate; 2) the superthermal metallic state is as or more stable than typical photoinduced metallic phases; and 3) the absence of hot electrons accompanying the insulating UO_2 excited state. This heterogeneous, non-equilibrium, Fröhlich BEC stabilized by a Fano-Feshbach resonance therefore continues to exhibit unique properties.

I. INTRODUCTION

Nine decades after their original prediction and six after superfludity was found in liquid ^{4}He dilute atomic gas Bose-Einstein condensates were produced in the laboratory by cooling their constituent particles into the nanoKelvin regime.[1-3] An interesting alternative, and one possibly more amenable to applications because of its wider range, may be non-equilibrium "Fröhlich" Bose-Einstein Condensates (BEC) of quasiparticles created by excitations in condensed matter.[4] These were proposed fifty years ago for collective phonons in polarizable dielectrics. An excess population of the excited state occurs because its relaxation is retarded when the energy of the phonon is in proximity to the chemical potential, with the coherence a spontaneous product of the Coulomb force-mediated interactions. The generality of this scheme – other long range forces could be equally effective in synchronizing oscillating charge (and spin) – is demonstrated by the assignment of unusual coherence and related properties in Bi to this type of mechanism.[5-8] Is this concept applicable to the other nonequlibrium BECs composed of magnons[9, 10] and exciton-polaritons?[11-14] Exciton-polaritons also accumulate in a narrow energy band because of an energy resonance that retards relaxation.[14] Similarities with conventional atomic gas and in particular fermionic BECs and the significance of their associated chemical potentials to the condensate phase diagram and pair formation have also been described.[15]

A species missing from this quasiparticle menagerie is polarons, which are of great interest because they possess mass, charge, spin, and much higher energies. Polarons are also important because, coming from the other direction, exotic superconductivity and the associated Bardeen-Cooper-Schrieffer (BCS) condensates, pseudogap, and possibly BEC states[16] originate in the polarons in partly filled Mott insulators.[15] Although three decades after the discovery of high temperature superconductivity in cuprates consensus on the mechanism is still absent, over the last several years there is nevertheless a convergence of several themes. One is the coupling with atomic gas Bose-Einstein condensates via the condensate phase diagram. Another is the stabilization afforded by exchange via, e.g., Fano-Feshbach and similar resonances.[17, 18] In fermionic atomic gas BECs this is between atoms and the diatomic molecule, in contrast to exotic BCS condensates where the postulated exchange occurs between two different electronic bands at the Fermi level.[19, 20] A third common basis is the importance of the chemical potential or related parameters in the properties of both ground state and non-equilibrium condensates.

With respect to the polaron, Fröhlich BEC problem, we have reported[21, 22] a large number of unusual or unique results from structural and spectroscopic experiments on the U 5*f* Mott insulator UO_2 that are best interpreted as demonstrating that polarons in UO_2 form non-equilibrium condensates. The polarons created by O-doping of UO_2 give UO_{2+x} that retains the fluorite structure up to x=0.33–0.5. The crystallographically single phase compounds in this range are U_4O_9 and U_3O_7. For intermediate stoichiometries clustering of the adventitious O causes the material to exist as nanophase separated UO_2:U_4O_9 and U_4O_9:U_3O_7 mixtures. Polarons are also created by photoexcitation of UO_2 via the metal-to-metal charge transfer transition, creating transient U^{5+}-U^{3+} pairs in which the U^{5+} appears behave analogously to O-doping. The instability of U_2O_3 implies that the U^{3+} may simply disperse. The combination of XAFS, x-ray pair distribution function (pdf) analysis, and neutron pdf has shown that the polarons in UO_{2+x} are tunneling polarons.[23, 24] The distances over which the atoms hop are, however, far too large for conventional tunneling, exceeding those in cuprates[25] by at least an order of magnitude. These polarons from both O-doping and photoexcitation aggregate and self-organize into CPQPs possessing exceptional coherence, stability, and other collective effects persisting even up to ambient temperature. Their non-equilibrium condensate-like properties would then be the culmination of the phonon-coupled, synchronous charge transfer displayed by related systems.[26,

[27] These comprehensive structural results have been interpreted in terms of a real space description in which the non-degenerate charge transfer and atom displacements of the tunneling are synchronized over the entire domain to give the coherence within the CPQPs. This coherence is enhanced by a Fano-Feshbach resonance[15, 17, 18] that connects the U(IV,V) ground state open channel and U(IV,VI) excited state closed channel species that are preferred at the opposite ends of the vibrational excursion of a special [111] phonon.[28]

Time-domain optical pump-optical and THz probe experiments on $UO_{2.0}$ and electron paramagnetic resonance (EPR) spectroscopy measurements on O-doped UO_{2+x} have identified multiple states accruing to the CPQP and shown that at least some possess extraordinary coherence and collective properties. An outstanding question, however, is the electronic structure. Herein we delineate the response of the Mott gap to O-doping by combining the O X-ray Absorption Spectroscopy (XAS)[21] and Non-resonant Inelastic X-ray Scattering (NIXS)[29] with Resonant Inelastic X-ray Scattering (RIXS), and to photoexcitation via time resolved photoemission.[30] In addition to the analogies with atom gas Bose-Einstein condensates, the identification of these states and their connections demonstrates the equivalence of this real space scenario with two-band, coherent-exchange, superconductivity mechanisms.[19, 20] These experiments also continue the established pattern of identifying unique behavior in $UO_{2(+x)}$, in this case the properties of the electronic states with doping and the relaxation and adoption of stable states after photoexcitation.

II. RESULTS AND DISCUSSION

We will first examine the polarons caused by O-doping, beginning with the electronic states of U-O standard compounds using O XAS and RIXS to identify any trends and patterns and determine the accuracy of calculations. The calculations can then be used to predict the O-addition mechanism and resulting types of structures and their electronic states. An important constituent of the O-doped UO_{2+x} system is the U_4O_9 and U_3O_7 fluorite-based structures obtained by neutron scattering that do not show tunneling polarons and will be referred to as "static". The spectra from these standards will be compared against those of U_4O_9 and U_3O_7. If these show electronic states outside the range of those expected empirically and predicted theoretically we can infer that they are correlated with the other unique experimental results on this system, i.e., the tunneling polarons derived from x-ray measurements and collective aspects of the spin that we have attributed to a CPQP whose constituent particles have undergone condensation. For U_4O_9 and U_3O_7 this would be the CPQP composed of the fixed concentration of tunneling polarons produced by O-doping. We will subsequently present time-resolved optical-pump photoemission-probe results that will elucidate the density-of-states of the CPQP composed of photoexcited polarons that has shown exceptional coherence, multiple phases, and greatly extended lifetimes. Comparing the results of the two types of experiments on the two types of polarons will identify commonalities between the condensed CPQPs that will help determine the extent to which they are related. The spectra will also be discussed in the context of the various resonances that could promote and stabilize condensation. The DOS of the CPQP will be examined for consistency with and additional information on the synchronization-coherence mechanism that we have postulated from the structure experiments. Finally, novel properties of the CPQP obtained from the new data will be described.

A. O XAS and RIXS of relevant standard compounds

The electronic structure and associated x-ray spectra of uranium oxides and related compounds have been extensively studied both experimentally and theoretically and are well understood. A

component of these studies has been XAS that contains information on the unoccupied electronic states. In UO_2 these are the states of the Upper Hubbard Band (UHB) above the Mott gap. Figure 1A shows the O XAS of: UO_2 that is cubic with U(IV); U_3O_8 that is layered with two distinct U(V) and (VI) sites; α UO_3 that is layered and U(VI)[31-34]; and the molecular complex $Cs_2UO_2Cl_4$ that possesses the U(VI) trans dioxo moiety that is inherent to the higher U valences and defines the oblate local geometry that is the basis for layering.[35] Because of the symmetry relationship between the cubic U site of UO_2 and the quasi-octahedral site of the layered materials and uranyl complexes these spectra for both geometries consist of two peaks. The lower energy peak is of predominantly U 5*f* character, and is well separated and distinct from a higher energy peak that is predominantly of U 6*d* character.[36-38] The energies of these peaks are ~533.5 eV and ~538-540 eV, with those of U(IV) higher than U(VI) by, respectively, ~0.5 and ~1.5 eV. The valley between these peaks decreases with increasing valence by ~1.5 eV, but in a more complicated way because of variations in the peak widths and the presence of additional spectral features. These two peaks exhibit comparable spectral weights throughout this series, although the sensitivity of the U absorption to its environment is such that their relative amplitudes can vary somewhat between different batches of material (Fig. S1[39]). The heights of the peaks can be suppressed by self-absorption when measured by fluorescence yield, with the correct amplitudes given by NIXS (Fig. S2).[21] The accuracy of NIXS is also potentially better because it was performed with 10 keV x-rays that penetrate several microns into the sample and is insensitive to modification or degradation of the surface.

The occupied O 2*p* and the U 5*f* states[73] of UO_2 and U_3O_8 have been probed by valence-to-core 3*d*5*f* RIXS at the U M_5 edge[74] measured at 3552 eV (Fig. 1B). Complementary to the XAS, these constitute the Lower Hubbard Band (LHB) below the Fermi level. For UO_2 the separation between the broad O 2*p* band and the narrower U 5*f* one is 2-2.5 eV. Relative to UO_2 the peak and leading edge of the O 2*p* states of U_3O_8 are ~2eV higher. This value for the leading edge of UO_2 is, however, somewhat arbitrary because it is not smooth but exhibits significant structure at or slightly above the noise level that makes it vary from 2.5 eV near its maximum amplitude to 1.5 eV near the baseline. The peak of the U 5*f* states is only ~ 0.5 eV higher for U_3O_8 relative to UO_2. The overall separation between these is therefore substantially reduced and the O 2*p* and U 5*f* states in U_3O_8 are close to overlapping. It is not clear, however, if the leading edges of the U 5*f* states share this behavior. It is somewhat ambiguous because the lower amplitude of the U_3O_8 5*f* peak makes it appear narrower and the noise at the baseline prevents determining if it extends to higher energy as the UO_2 peak does.

B. Calculations for relevant standard compounds and U_4O_9 and U_3O_7

Calculations with advanced treatments of the Hubbard U (the on site Coulomb repulsion) and spin-orbit coupling have identified the crystallographic structures as the lowest energy ones for the common uranium oxides and are in agreement with other parameters as well. As would therefore be expected, the electronic structures found by the various calculations are also quite accurate with respect to the O XAS spectra of the standard compounds (SI and Figs. S3-S6). The calculated density of states (DOS) (Fig. 2A and S4) gives results for UO_2 very similar to those already cited.[31, 33, 36] The optical gap of ~2 to ~2.4 eV is slightly on the high side but within the error of the measurements.[75, 76] In addition to the assignment of the features, extended analyses of UO_2 show that the width and complexity of the peaks of its spectrum are the result of a combination of crystal field, Coulomb, and multiplet splitting effects (SI and Fig. S3). Increasing valence should therefore cause them to become narrower,[31, 33, 36, 77] a prediction that is confirmed with this set of compounds. Because of this increase in width the lower edge of the Upper Hubbard Band (UHB) does not track the shift of the peak. Instead, the front edges of the UHB

for UO_2 and UO_3 are at the same energy with U_3O_8 a few tenths of an eV higher (Fig. 1A). This effect as well as the complementary broadening on the high energy side of the unoccupied 5*f* states is produced in the detailed treatment of the spin-orbit coupling (Table S1 and Fig. S3).

The calculations also match the experimental results for the occupied states of the two standards where we have RIXS spectra, UO_2 and U_3O_8. The accuracy of the calculations for U_3O_8 is better for some functionals than others. Our LDA+U calculation and the one with the HSE (Heyd-Scuseria-Emzerhof) functional show the wide gap between the occupied O 2*p* and U 5*f* states in UO_2 (Figs. 2A and S4). In U_3O_8 an extension of the O 2*p* states (Fig. S6) gives the reduction of this O 2*p*–U 5*f* gap observed in the experiments. The LDA+U also matches the data in that the UO_2 5*f* states are broader than in U_3O_8. In addition, the calculations show relatively steep slopes on the edges of the DOS, suggesting that the broader DOS found in the RIXS may simply be an experimental effect. If so, the peak energies will give the behavior of the states more accurately than the edges of the spectral features.

The accuracy of the various calculations that were successful for the standards gives assurance that the di- and quad-interstitial structures and DOS for the mixed valence fluorites U_4O_9 and U_3O_7 obtained with LDA+U[78] are valid. These defectstructures are very similar locally to the long-standing cuboctahedron model derived from extensive analysis of neutron diffraction.[79-84] In both descriptions adventitious O is added into the cubic hole sites accompanied by the displacement one or two neighboring cube vertex O atoms into adjacent cubic holes. U_3O_7 uses the same motif, differing from U_4O_9 in the longer range ordering of the cuboctahedron or alternative less ordered defect structures. The U sublattices of U_4O_9 and U_3O_7 are mostly conserved from that of UO_2, and the lattice constants differ by almost negligible amounts. These calculated structures are in excellent agreement with the static ones obtained from neutron scattering[85] in which the charge inhomogeneities are small polarons. These structures are relatively minor perturbations on UO_2 that maintain its basic cubic-radial site symmetry with no U-O bonds below 2.2 Å and thus no formation of U(VI)-oxo species or layers. The neutron scattering data from U_4O_9 therefore does not find the tunneling polaron or other evidence of the CPQP and its condensation, in contrast to the EXAFS and x-ray pdf measurements that do. In addition to being unobserved by neutron scattering, the CPQP is not found in any of these calculations. The calculations are therefore limited to reliably providing the electronic states for this static description of the structure with small instead of tunneling polarons.

C. RIXS, O XAS, and NIXS measurements of U_4O_9 and U_3O_7

The corollary to the consistency of these results from the neutron scattering and electron structure calculations is that if the experimental spectra do not agree with the calculations it will be because they are measuring the CPQP as seen by the hard x-ray structure probes, either because it is intrinsic or being excited by the probe beam. The calculations and experiments do correspond well for the occupied states of the LHB (Figs. 1A, 2A, and 2B). The LDA+U calculations for U_4O_9 and U_3O_7 give an ~0.7 eV increase in the edge of the O 2*p* states and ~0.25 eV increase in the U 5*f* states for the former and slightly larger for the latter (Fig. 2A). The increase in the U 5*f* peak energy is ~0.5 eV, with some uncertainty because of the width of the peak for UO_2. These values are within the error of the 1.3 (O 2*p* band edge) and 0.4 eV (U 5*f* peak) values (Figs. 1B and 2B) observed in the RIXS of U_4O_9. As with U_3O_8, it is difficult to discern differences in the U 5*f* band edge because of the noise level at the baseline. Empirically, relative to U_3O_8 the shift in the O 2*p* states of U_4O_9 is a few tenths of an eV less and the U 5*f* states is the same (Fig. 1B), so they fall within the bounds set by this standard. Therefore the

occupied states conform to the expectations for the static structure and do not display any unusual or notable features.

In contrast, however, Figures 1A, 2A, and 2C (and *cf.* S2 for U_3O_7) show that the O XAS spectra and by implication the unoccupied states of U_4O_9 and U_3O_7 decidedly fail to match the calculations or fall within the empirical bounds. They do not even duplicate the basic two peak structure common to all of the other spectra that originates in the separation of the U 5*f* and 6*d* states of the UHB. The highest amplitude peaks in the O XAS of U_4O_9 and U_3O_7 occur over the same energy as the 6*d* final states for the higher U valence compounds (Fig. 1A), but this is in part because they are much wider. Below this peak, the leading edges of the UHBs of U_4O_9 and U_3O_7 are, respectively, 1.5-2 eV and 2-2.5 eV lower in energy than the edge of the U 5*f* peaks of U_3O_8, and UO_3 and 1.2 and 1.8 eV lower than the U 5*f* edge of the NIXS of UO_2 (Fig. 2C). In addition to these empirical comparisons, the calculations obtain only a 0.6 eV decrease in the energy relative to the UHB edge of UO_2. Furthermore, the shapes of the U_4O_9 and U_3O_7 spectra differ substantially from those of the standards. The NIXS[21] with its accurate amplitudes (Fig. S3) shows that the U 5*f* peak that is at 533.2 eV for UO_3 but at 531.2 eV for U_3O_7 has transferred most of its spectral weight to the higher energy one. For U_4O_9 this transfer of weight is so extensive that the lower energy peak is only a shoulder on a very broad absorbance. The absorbance minimum between the U 5*f* and 6*d* spectra is also modified by these changes so that it now occurs at the energy of the U 5*f* peak from the standards.

There are two more notable results. First, the U_4O_9 spectrum is distinct from that of U_3O_7 (Fig. S7) and is not a sum of those of UO_2 and U_3O_7. This indicates that U_4O_9 and U_3O_7 possess different states. Second, the U_4O_9 and U_3O_7 spectra differ radically from those of U_3O_8, UO_3, and $Cs_2UO_2Cl_4$ despite the EXAFS showing U-oxo neighbors with 1.7-1.8 Å U-O distances in all of these compounds. In addition, these differences are specific to the UHB. These differences for U_4O_9 and U_3O_7 are therefore caused neither by the trans dioxo structural moiety nor the core hole (Fig. S8). They must therefore originate in some other factor that would be unique to the mixed valence fluorite compounds. Small or unaggregated, localized polarons[75] as have been proposed to be thermally activated in UO_2[75] – or possibly promoted by pressure that lowers their formation energy[86] – contract the band gap by amounts close to those calculated for U_4O_9 and U_3O_7. These amounts are, however, much less than the values found in the XAS. The structure and speciation of the charge inhomogeneities must therefore be substantially more radical to give these spectra. It is specifically the unoccupied states above the Fermi level that are affected while the ones of the LHB match the calculations. This indicates that these results are not a small polaron of the static cuboctahedron or di- and quad-interstitial structures but a novel state. Such a state would originate in the observed CPQP.[21]

D. Additional characteristics of XAS and DOS of the Coherent Quantum Phase of the polarons created by O-doping

The large reductions in the energies of the features in the XAS of U_4O_9 and U_3O_7 demonstrate that the band gap is much less in the CPQP than the measured or calculated ones for other U oxides or the calculated ones corresponding to the static, neutron scattering derived structures of U_4O_9 and U_3O_7. Obtaining an exact value is difficult because the Fermi level is not defined in the XAS measurements and the extent of experimental broadening of the band edges is uncertain. We can, however, align the U 5*f* peaks of the RIXS and XAS spectra with the corresponding maxima in the DOS and the midpoint of the XAS of UO_2 with the calculated band edge (Fig. 2B). Using points between the baseline and midpoints gives gaps close to the measured and calculated ones to serve as a basis for evaluation. We start by comparing the shifts of the spectral

features against those reported for UO_2 and U_3O_8. The XAS shows that the edges of the unoccupied U 5*f* states of UO_2 and U_3O_8 are quite close or possibly even somewhat less for UO_2 because of the width of its U 5*f* XAS peak. The reduction of the gap from 2.2 eV for UO_2 to 1.8 eV gap of U_3O_8[87] must therefore result from the increase in energy of the occupied U 5*f* states of U_3O_8. This implies that the peak values are a better guide to the behavior of the LHB found by RIXS than the band edges. We will then assume that the occupied U 5*f* states are wider than found by the fit of the U_3O_8 RIXS and that the band edge of the LHB shifts by the same amount as the peaks. This gives the correct gap and validates the posited alignment of the spectra. The 1.5-2 eV decreases in the leading edges of the XAS, even without the possible 0.25 eV increase in the occupied U 5*f* state, therefore indicate that the band gap in the CPQP is at most only a few tenths of an eV.

A caveat in this interpretation of the spectroscopy experiments is that bulk conductivity measurements of U_4O_9 have shown that it is an insulator.[88] The different types of experiments, however, probe different effects and also possess different sensitivities to, e.g., the surface structure. There is also the possibility that the CPQP is caused or triggered by a significant photoinduced polaron density from the probe beam. Another crucial characteristic is that, after normalization of the amplitudes of the different spectroscopies against the calculated DOS (Fig. 2A), the UO_2 NIXS spectrum ends abruptly (Fig. 2B) but the XAS of UO_2 gradually tails off over the same range. This tail intersects the RIXS at a few percent of the height of its U 5*f* peak (*cf.* Fig. 2E with U_3O_7). The spectra of U_4O_9, and U_3O_7 display these tails as well. Although this could be homogeneous spectral broadening, the convergence of these tails for all three UO_2, U_4O_9, and U_3O_7 spectra implies that it at least partly reflects actual electron states. This difference between the NIXS and XAS suggests that the tail could be caused by a surface-proximity phenomenon over the top few hundred nm (*cf.* Raman spectra in Fig. S9). The alternative is a threshold effect in which the local density of the polarons with the more penetrating 10 keV x-rays is below that required for formation of the CPQP. We observed a similar threshold in our optical pump-THz probe measurements.[22] Supporting this second possibility is that the U L_3 EXAFS of UO_2 also showed no evidence of the CPQP. O-doping of UO_2 to U_4O_9 and U_3O_7 therefore substantially reduces or possibly even bridges the Mott gap. This is accomplished principally by creating excited states that fill in the Mott gap downwards from the UHB. A tail off of the UHB gives a small but finite DOS at the intersection with the LHB, following which the DOS increases rapidly with increasing energy after this node or chokepoint (Fig. 2E).

The overlap of the UHB and LHB has probably been observed previously. In a previous measurement of the XAS of UO_2[33] the fluorescence yield O K edge XAS is that for UO_2 with the high amplitude of the 532 eV peak characteristic of single crystal samples (Fig. S1, from the same UO_2 boule as in this reference). However, the total electron yield spectrum distinctly resembles ours of U_4O_9 in terms of the number of features, their energies, their relative amplitudes, and the shift of the leading edge of the UHB relative to UO_2. This discrepancy would be explained by the surface of the UO_2 having oxidized to U_4O_9, with the oxidation not penetrating deeply into the sample. The U $4d_{5/2}$ spectrum where the final state is the U 5*f* levels of the UHB consists of a single peak that is at least a factor of two wider than any of the peaks in all of the other spectra. This was interpreted as Lorentzian broadening. However, the calculated U 5*f* states and optical response exhibit the same widths as the other states and the shape of the lower 30% of the peak is more linear than curved. The clear extension of the tail of the experimental data below the assigned Fermi level, in contrast to the calculation where the states stop at the UHB edge, could therefore be the same result for excitations into the U 5*f* states that we have described. This would corroborate our finding that the occupied/LHB and

unoccupied/UHB U 5*f* states in the doped systems overlap at a chokepoint or node in the DOS in a semimetal configuration in an x-ray measurement.

These states that differ from the calculations and the behavior of the standards would result from our proposed aggregation and self-organization of the polarons into a CPQP. Its electronic states in this energy range are in the gaps of UO_2 and the neutron-scattering derived structures of U_4O_9 and U_3O_7. Probes and calculations limited to this static ground state structure therefore find relatively small deviations from UO_2 while probes sensitive to faster time scales[24, 89] – which include the x-ray experiments reported here – find the CPQP.[21, 22] The significance of dynamics in the structure in the form of tunneling polarons[21] is further corroborated by the changes in the XAS between ambient and liquid N_2 temperatures (Fig. 3). These show a transfer of spectral weight from the tail at the UHB edge to the U 6*d* and especially 5*f* states for UO_2 but increased amplitude over the entire region below the U 6*d* peak for U_4O_9 as well as other changes in relative amplitudes. Much smaller differences in these spectra from normal and superconducting cuprates were attributed to the redistribution of the mobile electrons between the available sites.[90] It would be consistent with the temperature dependence of the U L_3 EXAFS of U_4O_9 (and U_3O_7) that showed continuous fluctuations of the U-O distribution over a wide temperature range even in the absence of any crystallographic phase transitions.

E. DOS of the Coherent Quantum Phase of photoinduced polarons

Time-resolved photoemission measurements were performed[30] at 1.6, 3.1, and 4.7 eV. These would be transitions from the U 5*f* state into, respectively, the gap, the unoccupied U 5*f*, and the unoccupied U 6*d* states. The latter two, concomitant with the 40 fs wide excitation pulses, are shown in Fig. 2D. The fluences of 0.13-0.51 mJ/cm^2 at 4.7 eV correspond to 0.002-0.006 excitations/U in the top 1 nm. This range is comparable to the 0.009 excitations/Ta for TaS_2 that induce its insulator-metal transition[26] and is therefore sufficient to give collective effects. As with the other optical pump experiments we have performed on $UO_{2(+x)}$, these measurements also gave highly unusual results. The prominent features in the 4.7 eV excitation spectra are the Mott gap and the front edge of the unoccupied UHB 5*f* states of the static UO_2 DOS (Figs. 2A and 2D). This includes the lower fluences below the high-order relaxation threshold[30] whose relaxation therefore extrapolates to the slow component of the biexponential relaxation (5-7 ps over the fluence range). The state that gave the fast relaxation (4-0.6 ps) therefore makes only a minor contribution to these spectra. The areas of the 5*f* spectral feature in the UHB after subtracting the background are linear with fluence even over the range where the fast relaxation is a large component of the total (Fig. S10). This fast relaxation must therefore represent electrons distributed over the entire energy range, similar to what occurs with 3.1 eV excitation. Close inspection of the spectra (Fig. 2D) shows that the flat backgrounds bracketing the UHB 5*f* feature do increase over their entire range with increasing fluence. Nevertheless, consistent with the spectrum consisting primarily of the minimally modified gap and UHB of the UO_2 DOS, the overlap of linear fits to the logarithm of the leading edge of the 5*f* peak (Fig. 4A) demonstrates an absence of the hot electrons. These would typically give either mid-gap states[26, 91, 92] or the photoinduced metallic state of thermalized hot electrons residing in states above the Fermi level[6, 26, 27, 93, 94] or edge of the valence band even in filled insulators.[26]

The t=0 spectra with 3.1 eV excitation, with fluences from 0.7-3.2 mJ/cm^2 = 0.015-0.07 excitations/U in the top nm, are the converse of those at 4.7eV. The DOS of these excited states (Fig. 2D) are continuous and relatively flat over the full 3 eV monitored with no sign of features in the UHB U 5*f* region. This smooth, featureless DOS resulting from 3.1 eV excitation that extends several eV above the Fermi level is distinctly similar to those for the U_4O_9 and U_3O_7

DOS in this same energy range beyond the constricted intersection of the occupied states and tails of the unoccupied ones. These parallels in the DOS between the photo- and O-doped systems also extend to the 4.7 eV excitation that recapitulates the UO_2 DOS measured by NIXS and the calculations of UO_2 and the neutron-scattering derived structures of U_4O_9 and U_3O_7 through the leading edge of the unoccupied U 5*f* states.

The observed spectra would result from the excited electrons instantaneously forming the UO_{2+x} CPQP without atom displacements. A precedent would be the photoinduced formation of the charge density wave in TaS_2 which also forms faster than atomic motions, although in that case there is a delay for the relaxation of the initial nonthermal electrons.[26] Increased fluence increases the magnitude of this instantaneous, nonthermal DOS and also produces hot thermalized electrons whose temperature parallels the fluence (Fig. 4B). Like 4.7 eV, excitation at 3.1 eV was also shown to give biexponential relaxation, with an initial fast lifetime of ~4-0.22 ps for 0.71-3.2 mJ/cm^2 and a slow lifetime of 8 ps.[30] That the shapes of the spectra are retained even at fluences below the value where the fast relaxation is minor therefore indicates that it corresponds to the slow relaxation spectrum, which is the same result as with 4.7 eV excitation. This is corroborated by the ratio between its integrated areas for 0-1.5 eV and 1.5-3.25 eV being the same at all fluences (Fig. S10).[95]

Although this t=0 spectrum shows the expected metallic state[26, 95] typically observed in oxides,[96] its extended energy, relatively flat DOS, and the stability implied by its extended fluence independence and association with the slow lifetime resemble the behavior of graphene.[97] This is significant because, although this common response could be coincidental, we have now shown that the DOS of U_4O_9 and U_3O_7 also resemble that of graphene. Both UO_2 and grapheme show the shift of the UHB and consequent closing of the Mott gap that causes their DOS to descend to a narrow constriction at or near the Fermi level followed by a rapid increase immediately afterwards into the unoccupied states. Another similarity specific to the excited states of both is that thermalized electrons fill in this chokepoint off of the leading edge of the valence band to flatten the overall DOS to resemble a metal (Fig. 2C). We have already shown that the CPQP forms rapidly; the coherence coupled to the CPQP in $UO_{2(+x)}$ in time domain spectra is already at a maximum after the initial ¼ period of 250 fs, instead of the more typical half to one period from other materials.[26, 27, 98] Alternatively, the CPQP could form in domains where the transient U (111) interplanar separation is large and mimics the CPQP structure at the instant of excitation.[96]

The t=0 DOS produced by 3.1 and 4.7 eV excitation are opposites, as is the absence of a response with 1.6 excitation.[30] The former promotes electrons into the unoccupied states of the CPQP that forms concomitantly, the latter into those of the static, neutron-scattering derived UO_2 structure. That this is not an effect of the fluence is demonstrated by the lifetimes[30] and the absence of the 5*f* UHB feature with 3.1 eV excitations. Energy dependence in the initial response to intense fs optical pulses is antithetical to the current depiction of the photon impulse promoting hot electrons into a continuous, nonthermal energy distribution.[26, 95] This result for UO_2 is, however, obligatory since excitation at these energies already has given different results when probed by reflectivity. Reflectivity gave the CPQP when excited at 3.1 but not 4.7 eV,[21] just as it also gives the CPQP-type result here.[21]

F. Spectroscopy results and the CPQP

Recapitulating, introducing charge inhomogeneities into UO_2 that form polarons, either by the addition of O to UO_2 to form U_4O_9 and U_3O_7 or by photoexcitation specifically into the U 5*f* states of the UHB, results in:

- only minor modifications to the occupied U 5*f* states of the LHB that easily conform to the bounds set by the related standard compounds and calculations;
- when probed by XAS or optical pump-photoemission, a substantial reduction or possibly even elimination of the Mott gap via novel states that do not conform to the patterns established by standard compounds and calculations and which are extensions of or connect with the UHB of UO_2.

The behavior of the gap inferred from this combination of RIXS and XAS can be compared with direct optical absorption measurements of UO_2 at high temperature[75] or pressure.[86] Such a comparison demonstrates that these novel states are not the postulated small polarons that reside in the slightly modified structures[78, 99, 100] found by neutron scattering [79-84] or the result of similar small compressions of the U-O bonds. Instead, given the correlations with our previous experiments, we conclude that these novel states are either the CPQP itself or its signature within these measurements that show the electronic structure.

The rising absorption in the XAS implies that the DOS increases after the gap or chokepoint near the Fermi level (Fig. 2C) whereas the DOS from photoexcitation at 3.1 eV is relatively flat (Fig. 2D). However, both the XAS of stationary U_4O_9/U_3O_7 and time-resolved photoemission of transiently photoexcited UO_2 show that the number of states/electrons remains elevated through the UO_2 gap region and across it into the original unoccupied states of UO_2. The immediate, unrelaxed, nonthermal photoelectron spectrum for all materials is relatively flat through the photon energy, thermalizing within a few tens to at most a few hundred fs. In UO_2, however, it persists for multiple ps, demonstrating that this distribution of electrons that would normally correspond to temperatures of tens of thousands of K already is the final state. It is therefore a property of the CPQP, with the states occupied by the electrons being actual rather than virtual ones. Insofar as this pattern of states is found for U_4O_9 and U_3O_7, these could be the same. In that case the DOS of the CPQPs are the same or at least closely related regardless of whether the CPQP originates in O-doping or photoexcitation. It follows that the CPQPs observed in x-ray measurements of U_4O_9/U_3O_7 and photoexcitation are also the same or closely related. Likewise, the final state is attained immediately with 4.7 eV excitation, although in this case it is the electron distribution of the original UO_2. Assuming that the CPQP from photoexcitation is the same as from O-doping, the absence of the constriction in the DOS just above the Fermi level after 3.1 eV excitation would result from the continuous replenishment of the electrons in the virtual states in the constriction from the reservoir of nonthermal ones. This process would also give some thermalized electrons on the leading edge of the U 5*f* peak of the LHB.

Previously, using optical reflectivity and time domain THz probes we found greatly extended lifetimes and coherence for states that we attributed to the CPQP. The time resolved photoemission now shows electrons with energies 2-3 eV above the Fermi energy persisting for an extraordinary 6-9 ps at ambient temperature[30] (Fig. S10). (And possibly μs below 60 K if this is the same state observed in the optical pump-reflectivity probe experiments.[21]) This can be understood for the static UO_2 5*f* states obtained with 4.7 eV excitation because, as we have posited,[30] relaxation requires returning across the barrier of the full Mott gap (Fig. 2D). The absence of a gap in the DOS with 3.1 eV excitation obviates this rationale for the CPQP. The continuity in energy in the absence of a gap would be expected to accelerate the relaxation of the photoinduced CPQP relative to the UHB states of UO_2. Instead the relaxation times associated

with the two states are within <50% of each other.[30] Exceptionally long lifetimes are, however, a basis for nonequlibrium BECs because the condensate lifetime cannot be longer than that of its constituent quasiparticles; extended lifetimes are required for condensation. Inversely, their lifetime may be extended by their participation in the condensate. We consider the CPQP in O-doped U_4O_9 and U_3O_7 with tunneling as static because the polaron concentration does not change with time. However, it was found in cuprates that x-ray probes provide instantaneous snapshots of the multisite structure associated with the upper vibrational states of the double well because their fast interaction time causes their energy to be broadened.[24, 89] The x-ray probes themselves may therefore provide sufficient energy to populate levels coupled to the tunneling, which would account for some of the differences between these spectroscopic and other types of measurements.

G. Identification of condensate-stabilizing resonances

The non-equlibrium, exciton-polariton and phonon condensates form because their quasiparticle relaxation is inhibited. The excited quasiparticles accumulate in the first state above the relaxation bottleneck to give the nonthermal population distribution that subsequently attains coherence. Underlying these extended lifetimes are specific resonances. For phonons it would be the proximity of the excited phonon energy to the chemical potential.[4, 5] For exciton-polaritons it is the proximity of the exciton and cavity photon energies around k=0 and their avoided crossing that creates the minimum in the lower polariton band.[14] For the dilute atomic gas fermion-diatomic molecule boson systems it is the matching of the continuum of the fermionic potential with the energy of the molecule that activates their exchange via the Fano-Feshbach resonance.[15, 17] An analogous resonance has already been demonstrated in UO_2 by the excitation energy dependence of the coherence, lifetimes, and the formation of the photoexcited CPQP.

The role of resonance and the microscopic themes in non-equilibrium Fröhlich BECs and their specific contributions to the UO_2-system CPQP are elucidated by examination of the generic potentials of two state systems. The polarons on the apical O in cuprates tunnel between the two halves of a symmetric, degenerate, double well potential because the two structures involved are identical[24, 25, 101, 102] (although it is possible that the polarons in the CuO_2 planes are more complicated[87, 103]). An asymmetric double well would have been superfluous because of the assumption that the functionality originates in the ground state phase at all temperatures. In contrast, the two species involved in a non-equlibrium condensate are non-degenerate by definition, resulting in an asymmetric double well potential composed of the ground and excited quasiparticle states (Fig. 5). In this diagram the configuration of the overlapping potentials typically used for photoexcitation as well as to depict the fermionic atom gas condensate Feshbach resonance[15] is unfolded into a double well depiction. The energies are for the constituent atoms or quasiparticles of the condensate, and the distance coordinate will be for a pair of atoms that then also represents an order parameter giving the change in configuration. This same diagram between the two local minima can, however, also be viewed as a reaction coordinate. This is of interest because the fermionic diatomic molecule condensate undergoes changes in its chemical speciation as part of its coherence mechanism, as we have also proposed for the UO_2-system CPQP. The important component of a double well potential is the barrier, whose height and width determine the ease of exchange between the two halves. Phonon and exciton-polariton condensates depend on a high barrier that is difficult to cross (Fig. 5A), resulting in the accumulation of particles in the excited state that subsequently condense. However, since in the Feshbach resonance the continuum energy of the atoms equals the energy of the molecule, the barrier for the diatomic molecule to split is zero (Fig. 5B) with a smooth conic intersection of the two potentials instead of a peak or cusp.[104] In the absence of continuous

input from an external energy source the fermionic atom gas condensate must therefore retain the excess energy of the excitation, ΔE, while remaining coherent in order to continuing exchanging with the molecular one.

In the analogy between the UO_2-system CPQP and the fermionic gas condensate isolated polarons which would be the continuum state. The open channel is the weakly paired, spin triplet, fermionic U(IV,V) polarons in the U_4O_9-like domains that have been shown[99, 100] to be more stable than isolated polarons. The bosonic U(IV,VI) excited singlet state is the strongly paired closed channel. Relaxation is inhibited and the nonthermal population and condensation are favored when the chemical potential is near the energy of an excited phonon,[4] although this derivation is not specific and should apply equally well to any system with oscillating dipoles. Because UO_2 is an insulator the chemical potential is close to the midpoint of the gap. Since the states of the CPQP span the gap, or at least the measured DOS is large at the midpoint of the calculated gap for U_4O_9, this condition is met. Insofar as polarons maximize the atom displacements and polarizability they also fulfill this second criterion for strong coherence enhancement. In addition, the energy of the U_4O_9-like U(IV,V) cluster has been calculated to be 2.2 eV below that of the separated U(V)-O defects that would be the continuum or free polaron level.[78] Remarkably, this is almost exactly the difference between the centers of the spectral features that would be the occupied U 5*f* (Fig. 2B) and the lowest energy unoccupied (Fig. 2C) states in U_4O_9 . This proximity of the excited U(IV,VI) state energy to that of the continuum is the condition for the Fano-Feshbach resonance. The resonance for the CPQP of the UO_2 system therefore also belongs to the Fig. 5B scenario. The U(V) fermions are in the deeper minimum on the left and the U(IV/VI) bosons the one on the right at the longer U-U distance that accommodates the terminal U(VI)-oxo moieties. Although it is an open question if the relaxation from the excited state can still be retarded in the absence of a barrier, U_4O_9 and U_3O_7 fulfill the criteria for non-equlibrium condensation.

H. Correlation of the DOS with the proposed coherence mechanism

These new results in combination with our previous ones provide details on the underlying mechanism in energy-momentum space that complement the previously described real space scenario. They indicate that it is direct and does not involve suppression of competing orders such as the antiferromagnetism of UO_2.[22, 105] The x-ray and neutron structure measurements[21, 106] have identified the specific tunneling polarons that define the asymmetric double well. The polarons tunnel between the open channel fermion and closed channel boson states via the disproportionation reaction 2 U(V) ↔ U(IV) + U(VI),. The persistence of the condensate to high temperature is therefore a natural consequence of its origin as an excitation. Coherence throughout the entire domain is attained through synchronization of the electron transfer and correlated rearrangement of the O ions that constitute this reaction via the relative stability of the U(IV,V) species at the short U-U distances on the compressive and U(IV,VI) ones at the long distances on the tensile side of the [111] phonon. This phonon is already known to be special, also being implicated in stress relief caused by various defects.[28, 107] The long range force that synchronizes and gives coherence to the polaron-containing domains for the UO_2-system CPQP is therefore at least partly elastic instead of solely Coulomb. Specific to UO_2 and its absence of an insulator-to-metal transition; UO_2 differs from related materials in that the fluorite structure does not have a preferred orientation for adding O so that the calculation and neutron scattering structures of U_4O_9 are three dimensional. The layered U(IV)-(VI) structure that is the excited state displays the alternating valence that constitutes a charge-density wave, inverting the typical energies of the insulating and metallic states. In addition, another possible reason for the differences in the response to different excitation energies is that the excited state produced by

3.1 eV but not 4.7 eV excitation could be coupled to the U [111] phonon. This would be analogous to phonon-driven enhancement of electron correlation in cuprates[108] that has recently also been postulated for C_{60}.[109]

The electronic structure of the CPQP maps directly onto this real state model. The CPQP is not the minor perturbation of UO_2 predicted by calculations and found by neutron scattering. Instead it is a different species of UO_2 that originates in widespread collective behavior. Its wide dispersion could result from combining the two strongly coupled parent states via the tunneling.[24] The tunneling is another signature of a condensate, since it is far too long a distance for conventional tunneling but small within the superfluid[8] tunneling regime. In addition, the energy overlap of the ground U(IV,V) and excited U(IV,VI) DOS indicates that the dynamic exchange of their local atomic structures is also the coherent exchange between their electronic states that are separated at the Fermi level. This exchange enhances condensation in two-band descriptions of exotic superconductivity.[16, 110] Thus, in the UO_2 system the phonon that impels the hopping of the charges also promotes the coherence and resultant condensation, which is the opposite effect of it disrupting competing orders.[108, 109, 111] This coherent exchange, as a Fano-Feshbach resonance that amplifies exotic BCS[18, 19] and fermionic atom-molecule gas BEC condensates,[17, 112, 113] would be the origin of the coherence of the two states.

I. Additional properties of the CPQP and its condensate

The experimental results are thus best interpreted as demonstrating that the CPQP of the UO_2 system is a non-equilibrium, Fröhlich-type, polaron BEC. This poses the questions of whether it will have the properties of other condensates and if it will exhibit novel ones resulting from its constituent polarons having spin, charge, and mass. The extended lifetimes of the states after photoexcitation relative to other materials are remarkable. Even more incredible are the formations of the CPQP and the static UO_2 DOS from their respective excitation impulses within the 40 fs width of the measurement without the normal, initial, very short lived state of a continuous distribution of nonthermal electrons. The optical switching time is therefore essentially zero – or at least << the 40 fs width of the excitation pulse. This is consistent with the different outcomes with the different excitation energies in both the time resolved photoemission and the earlier pump-probe reflectivity; if the immediate responses to the excitation were the same at all excitation energies the system would have to evolve into the same intermediate states. This behavior extends to low energy as well in that excitation at 1.6 eV gave no response, although in other materials nonthermal electrons are created up to the excitation energy.

The partly filled bands above the chokepoint that form with 3.1 eV excitation and span the entire range of energy (Fig. 2E) could be described as a “superthermal” metallic state. These superheated electrons in other materials relax in a few tens to hundreds of fs into a normal metallic state with thermalized electrons. In photoexcited UO_2 they persist for two to three orders of magnitude longer and therefore are the stable state of the quasiparticles. Although the DOS of the state formed from 3.1 eV excitation resembles this one that typical of other materials, its lifetime demonstrates that the DOS it displays that is continuous for several eV consists of actual and not virtual states. These would be the states found for O-doped UO_{2+x}. Together with the result from the 4.7 eV excitation where the nonthermal state is also not observed, these results show that photoexcited UO_2 with its immediate switching does not give the prompt response to photoexcitation characteristic of other materials.

As stated, this CPQP state of photoexcited UO_2 persists for close to 10 ps or longer. The thermalized electrons (Fig. 4B) that may fill in and obscure the chokepoint in the CPQP DOS

found with O-doping could originate either directly or via relaxation from the superthermal metal population. That this pattern occurs with lower numbers but identical distribution even at low fluence is additional evidence for the stability of the CPQP in that it demonstrates that it forms spontaneously even from only a small quantity of O-doped or solely from photoinduced polarons. Although suggesting that electrons 3 eV higher than the Fermi level are a signature of a condensate would seem contradictory, this energy is an attribute of the electrons. It is not necessarily the energy of the condensate nor even its constituent polaronic quasiparticles. Since the atoms are tunneling through an anharmonic pair potential that traverses a 30% or wider range of U-O bond lengths it is perhaps not unexpected that they display a comparably wide range of electronic energies. In addition, there will be unusual constraints on the energy distribution because of the need to conserve it during the exchange between the ground and excited states.

Equally notable in the context of energy flow is the absence of hot electrons with 4.7 eV (and 1.6 eV) excitation (Fig. 4A). The immediate formation of the static UO_2 excited state is concomitant with the channeling of the excess electronic energy into other locations. As noted, since the hot electrons on the leading edge of the LHB with 3.1 eV excitation could originate in relaxation from the superthermal state it is possible that the energy of this photon impulse also does not heat the electrons. The most likely location for absorbing and redistributing the excess energy is the condensate itself. Its direct formation requires the conforming redistribution of the energy of the photoexcited electrons on a time scale that is a minimum of one to two orders of magnitude faster than normal relaxation via interaction with other electrons and lattice processes. Insofar as the difference between UO_2 and other materials is the presence of the real or incipient condensate, it is the most logical candidate for this novel property. Immediate heat transfer is a known consequence of superfluidity.

These results validate and extend our model for the CPQP and continue to highlight the preeminence of UO_2 as a system encompassing many of the current ideas about dynamic electron-phonon coupling as the origin of the polaron physics of Mott insulators and the convergence of Bose-Einstein and BCS condensates. We also note the observation that the Fano-Feshbach resonance that is not universal in non-equilibrium BECs is associated with a change in chemical speciation. This differentiates homogeneous non-equilibrium BECs where the quasiparticles are only perturbations of the ground state from heterogeneous ones that involve a chemical reaction and coherent exchange between the ground and excited state species. Additional novel properties may be found as this system is explored more thoroughly.

IV. MATERIALS AND METHODS

The materials and experimental procedures and modeling methods have been described previously.[21, 22, 29, 30, 74, 77, 78] The O K non-resonant inelastic x-ray scattering (NIXS) spectra of UO_2 and U_3O_7 were measured at the same time as the $O_{4,5}$ NIXS spectra previously reported[29] and therefore were from the same materials and used the same preparation and experimental methods.[114] The UO_2, U_3O_7, and U_4O_9 for the NIXS measurement were from the same materials as those used for a combined neutron and x-ray pair distribution function and U L_3 X-ray Absorption Fine Structure spectroscopy study.[21] The single crystal of UO_2 was from the same boule as used in previous ultrafast optical studies.[115] The sample of $Cs_2UO_2Cl_4$ was also from the same material used for in our $O_{4,5}$ NIXS report.[29] The O K fluorescence yield (FY) XAS measurements were also performed as reported previously[114] except that the UO_{2+x}/U_4O_9 spectra were measured on beamline 10-1 instead of 8-2. For the time resolved photoemission,[30] the number of excitations is calculated using the listed fluences, 1 nm thickness, optical densities of 1.2×10^5 cm^{-1} at 3.1 eV and 1.0×10^5 cm^{-1} at 4.7 eV,[116] density of 11.0 g/cm^3, and a formula weight for UO_2 of 270 g. No scattering correction was made.

Detailed information that reiterates the relevant content of the cited articles is included in the supplementary information[39].

Acknowledgments. Portions of this research were carried out at the Stanford Synchrotron Radiation Lightsource (SSRL), a national user facility supported by the U.S. Department of Energy, Office of Basic Energy Sciences operated by Stanford University, the Environmental Molecular Science Laboratory, a national scientific user facility sponsored by the Department of Energy's Office of Biological and Environmental Research and located at Pacific Northwest National Laboratory, and the Advanced Photon Source that is supported by the U.S. Department of Energy, Office of Science, Office of Basic Energy Sciences, Division of under Contract DE-AC02-06CH11357. Work at Los Alamos National Laboratory was supported by the United States Department of Energy, Office of Basic Energy Sciences, Division of Chemical Sciences, Geosciences, and Biosciences, Heavy Element Chemistry Program under contract DE-AC52-06NA25396, a Glenn T. Seaborg Institute graduate fellowship (J.A.B.), and the Los Alamos Laboratory Directed Research and Development Program. Los Alamos National Laboratory is operated by Los Alamos National Security, LLC, for the National Nuclear Security Administration of U.S. Department of Energy under Contract DE-AC52-06NA25396. PNC/XOR facilities at the Advanced Photon Source, and research at these facilities, are supported by the U.S. Department of Energy-Basic Energy Sciences, a Major Resources Support grant from NSERC, the University of Washington, Simon Fraser University and the Advanced Photon Source. Technical support staff at the ESRF provided assistance. J.J.K. and J.J.R. acknowledge United States Department of Energy, Basic Energy Sciences Grant No. DE-FG03-97ER45623, facilitated by the DOE Computational Materials and Chemical Sciences Network. P.S.B. acknowledges support from the United States Department of Energy Office of Basic Energy Sciences, Division of Chemical Sciences, Geosciences, and Biosciences, through the Geosciences Research Program at Pacific Northwest National Laboratory. G.T.S. was supported by the United States Department of Energy, Basic Energy Sciences, under grant DE-SC00008580 and by the Joint Plasma Physics Program of the National Science Foundation and the Department of Energy under grant DE-SC0016251.

References and Notes

[a]Institut Josef Stefan, Ljubljana, 1000, Slovenia, and Washington State University, Pullman, WA 99164, USA.

[b]Los Alamos National Laboratory, Los Alamos, NM 87545, USA.

[c]University of Washington, Seattle, WA 98195, USA.

[d]European Synchrotron Radiation Facility, Grenoble 38043, France.

[e]SLAC National Accelerator Laboratory, Menlo Park, CA 94025, USA.

[f]University of North Texas, Denton, TX 76203, USA.

[g]Uppsala University, Uppsala S-751 20, Sweden.

[h]Universidad Marista de Merida, Merida, Yucatan 97300, Mexico.

[i]Pacific Northwest National Laboratory, Richland, WA 99352, USA.

[j]Stanford University, Stanford, CA 94305, USA.

[k]CEA/DEN/DEC C.D. Cadarache, Saint Paul Les Durance 13108, France.

[l]University of New Mexico – Los Alamos, Los Alamos, NM 87544, USA.

[m]CNRS Ecole Centrale Paris, Chatenay-Malabry 99290, France.

[n]Synchrotron Soleil, Saint Aubin, Gif-sur-Yvette 91192, France.

*Corresponding author. Email: st3v3n.c0nrads0n@icloud.com

[†]Present address: Maria Curie-Sklodowska University, Lublin 20-031, Poland.

1. K. B. Davis, M. O. Mewes, M. R. Andrews, N. J. Vandruten, D. S. Durfee, D. M. Kurn, and W. Ketterle, *Phys. Rev. Lett.* **75**, 3969 (1995).
2. M. H. Anderson, J. R. Ensher, M. R. Matthews, C. E. Wieman, and E. A. Cornell, *Science* **269**, 198 (1995).
3. C. C. Bradley, C. A. Sackett, J. J. Tollett, and R. G. Hulet, *Phys. Rev. Lett.* **75**, 1687 (1995).
4. H. Frohlich, *Phys. Lett. A* **A 26**, 402 (1968).
5. O. V. Misochko, M. Hase, K. Ishioka, and M. Kitajima, *Phys. Lett. A* **321**, 381 (2004).
6. J. Faure et al., *Phys. Rev. B* **88**, 075120 (2013).
7. A. A. Melnikov, O. V. Misochko, and S. V. Chekalin, *J. Appl. Phys.* **114**, 033502 (2013).
8. O. V. Misochko, *J. Exp. Theor. Phys.* **118**, 227 (2014).
9. T. Nikuni, M. Oshikawa, A. Oosawa, and H. Tanaka, *Phys. Rev. Lett.* **84**, 5868 (2000).
10. S. O. Demokritov, V. E. Demidov, O. Dzyapko, G. A. Melkov, A. A. Serga, B. Hillebrands, and A. N. Slavin, *Nature* **443**, 430 (2006).
11. L. V. Butov, A. C. Gossard, and D. S. Chemla, *Nature* **418**, 751 (2002).
12. L. V. Butov, C. W. Lai, A. L. Ivanov, A. C. Gossard, and D. S. Chemla, *Nature* **417**, 47 (2002).
13. J. Kasprzak et al., *Nature* **443**, 409 (2006).
14. T. Byrnes, N. Y. Kim, and Y. Yamamoto, *Nature Phys.* **10**, 803 (2014).

15. Q. J. Chen, J. Stajic, S. Tan, and K. Levin, *Phys. Rep.* **412**, 1 (2005).
16. K. Okazaki et al., *Sci. Rep.* **4**, 4109 (2014).
17. E. A. Donley, N. R. Claussen, S. T. Thompson, and C. E. Wieman, *Nature* **417**, 529 (2002).
18. A. Bianconi, *Nature Phys.* **9**, 536 (2013).
19. A. Bianconi, *J. Supercon.* **18**, 625 (2005).
20. H. Keller, A. Bussmann-Holder, and K. A. Mueller, *Mater. Today* **11**, 38 (2008).
21. S. D. Conradson et al., *Phys. Rev. B* **88**, 115135 (2013).
22. S. D. Conradson et al., *Sci. Rep.* **5**, 15278 (2015).
23. S. D. Conradson, I. D. Raistrick, and A. R. Bishop, *Science* **248**, 1394 (1990).
24. M. I. Salkola, A. R. Bishop, S. A. Trugman, and J. M. Deleon, *Phys. Rev. B* **51**, 8878 (1995).
25. J. M. Deleon, I. Batistic, A. R. Bishop, S. D. Conradson, and S. A. Trugman, *Phys. Rev. Lett.* **68**, 3236 (1992).
26. L. Perfetti, P. A. Loukakos, M. Lisowski, U. Bovensiepen, M. Wolf, H. Berger, S. Biermann, and A. Georges, *New. J. Phys.* **10**, 197001 (2008).
27. I. Avigo et al., *J. Phys.-Condens. Matter* **25**, 094003 (2013).
28. L. Desgranges, P. Simon, P. Martin, G. Guimbretiere, and G. Baldinozzi, *JOM* **66**, 2546 (2014).
29. J. A. Bradley et al., *Phys. Rev. B* **81**, 193104 (2010).
30. S. M. Gilbertson, T. Durakiewicz, G. L. Dakovski, Y. Li, J.-X. Zhu, S. D. Conradson, S. A. Trugman, and G. Rodriguez, *Phys. Rev. Lett.* **112**, 087402 (2014).
31. F. Jollet, T. Petit, S. Gota, N. Thromat, M. Gautier-Soyer, and A. Pasturel, *J. Phys.-Condens. Matter* **9**, 9393 (1997).
32. M. Magnuson, S. M. Butorin, L. Werme, J. Nordgren, K. E. Ivanov, J. H. Guo, and D. K. Shuh, *Appl. Surf. Sci.* **252**, 5615 (2006).
33. S. W. Yu, J. G. Tobin, J. C. Crowhurst, S. Sharma, J. K. Dewhurst, P. Olalde Velasco, W. L. Yang, and W. J. Siekhaus, *Phys. Rev. B* **83**, 165102 (2011).
34. X.-D. Wen et al., *J. Electron Spectrosc.* **194**, 81 (2014).
35. R. G. Denning, J. C. Green, T. E. Hutchings, C. Dallera, A. Tagliaferri, K. Giarda, N. B. Brookes, and L. Braicovich, *J. Chem. Phys.* **117**, 8008 (2002).
36. X.-D. Wen et al., *J. Chem. Phys.* **137**, 154707 (2012).
37. X.-D. Wen, R. L. Martin, L. E. Roy, and G. E. Scuseria, *Chem. Rev.* **113**, 1063 (2013).
38. J. G. Tobin et al., *Phys. Rev. B* **92**, 045130 (2015).
39. See supplemental Material [url] for more detailed descriptions of the experimental and modeling/calculation methods and procedures and Figures S1-S10, which includes Refs. [40-72].
40. C. Greaves and B. E. F. Fender, *Acta Crystallogr. B* **28**, 3609 (1972).
41. V. J. Wheeler, R. M. Dell, and E. Wait, *J. Inorg. Nucl. Chem.* **26**, 1829 (1964).

42. T. T. Fister et al., *Rev. Sci. Instrum.* **77**, 063901 (2006).

43. T. T. Fister, G. T. Seidler, C. Hamner, J. O. Cross, J. A. Soininen, and J. J. Rehr, *Phys. Rev. B* **74**, 214117 (2006).

44. K. G. Tirsell and V. P. Karpenko, *Nucl. Instrum. Meth. A* **291**, 511 (1990).

45. F. M. F. Degroot, M. Grioni, J. C. Fuggle, J. Ghijsen, G. A. Sawatzky, and H. Petersen, *Phys. Rev. B* **40**, 5715 (1989).

46. C. Gauthier, V. A. Sole, R. Signorato, J. Goulon, and E. Moguiline, *J. Synchrotron Radiat.* **6**, 164 (1999).

47. K. O. Kvashnina, S. M. Butorin, P. Martin, and P. Glatzel, *Phys. Rev. Lett.* **111** (2013).

48. K. O. Kvashnina and A. C. Scheinost, *J. Synchrotron Radiat.* **23**, 836 (2016).

49. G. Kresse and D. Joubert, *Phys. Rev. B* **59**, 1758 (1999).

50. P. E. Blochl, *Phys. Rev. B* **50**, 17953 (1994).

51. G. Kresse and J. Hafner, *Phys. Rev. B* **48**, 13115 (1993).

52. G. Kresse and J. Furthmuller, *Phys. Rev. B* **54**, 11169 (1996).

53. G. Kresse and J. Furthmuller, *Comp. Mater. Sci.* **6**, 15 (1996).

54. S. L. Dudarev, D. N. Manh, and A. P. Sutton, *Philos. Mag. B* **75**, 613 (1997).

55. B. Dorado, B. Amadon, M. Freyss, and M. Bertolus, *Phys. Rev. B* **79**, 235125 (2009).

56. B. Meredig, A. Thompson, H. A. Hansen, C. Wolverton, and A. van de Walle, *Phys. Rev. B* **82**, 195128 (2010).

57. J. J. Rehr and R. C. Albers, *Rev. Mod. Phys.* **72**, 621 (2000).

58. J. J. Rehr, J. J. Kas, M. P. Prange, A. P. Sorini, Y. Takimoto, and F. Vila, *C. R. Phys.* **10**, 548 (2009).

59. P. S. Bagus, H. Freund, H. Kuhlenbeck, and E. S. Ilton, *Chem. Phys. Lett.* **455**, 331 (2008).

60. E. S. Ilton and P. S. Bagus, *Surf. Sci.* **602**, 1114 (2008).

61. P. S. Bagus, E. S. Ilton, and C. J. Nelin, *Surf. Sci. Rep.* **68**, 273 (2013).

62. K. G. Dyall, *J. Chem. Phys.* **100**, 2118 (1994).

63. H. J. Visscher et al., DIRAC, a Relativistic *ab initio* Electronic Structure Program, Release DIRAC08, http://dirac.chem.sdu.dk, (2008).

64. J. C. Slater, *Quantum Theory of Atomic Structure* (New York, McGraw-Hill, New York, 1960).

65. G. Burns, *Introduction to Group Theory with Applications* (New York: Academic Press, 1977).

66. S. Kern, C. K. Loong, and G. H. Lander, *Phys. Rev. B* **32**, 3051 (1985).

67. S. Kern, C. K. Loong, and G. H. Lander, *Physica B & C* **136**, 403 (1986).

68. Z. Y. Wu, F. Jollet, S. Gota, N. Thromat, M. Gautier-Soyer, and T. Petit, *J. Phys.-Condens. Matter* **11**, 7185 (1999).

69. D. Manara and B. Renker, *J. Nucl. Mater.* **321**, 233 (2003).

70. T. Livneh and E. Sterer, *Phys. Rev. B* **73**, 085118 (2006).

71. T. Livneh, *J. Phys.-Condens. Matter* **20**, 085202 (2008).

72. H. M. He and D. Shoesmith, *Phys. Chem. Chem. Phys.* **12**, 8108 (2010).

73. L. E. Roy, T. Durakiewicz, R. L. Martin, J. E. Peralta, G. E. Scuseria, C. G. Olson, J. J. Joyce, and E. Guziewicz, *J. Comput. Chem.* **29**, 2288 (2008).

74. K. O. Kvashnina, Y. O. Kvashnin, and S. M. Butorin, *J. Electron Spectrosc.* **194**, 27 (2014).

75. P. Ruello, K. D. Becker, K. Ullrich, L. Desgranges, C. Petot, and G. Petot-Ervas, *J. Nucl. Mater.* **328**, 46 (2004).

76. W. Siekhaus and J. Crowhurst, in *Actinides 2009*, edited by L. Rao, J. G. Tobin and D. K. Shuh (IOP Science, San Francisco, 2009), p. 012055.

77. P. S. Bagus, E. S. Ilton, R. L. Martin, H. J. A. Jensen, and S. Knecht, *Chem. Phys. Lett.* **546**, 58 (2012).

78. D. A. Andersson, G. Baldinozzi, L. Desgranges, D. R. Conradson, and S. D. Conradson, *Inorg. Chem.* **52**, 2769 (2013).

79. L. Nowicki, F. Garrido, A. Turos, and L. Thome, *J. Phys. Chem. Solids* **61**, 1789 (2000).

80. F. Garrido, R. M. Ibberson, L. Nowicki, and B. T. M. Willis, *J. Nucl. Mater.* **322**, 87 (2003).

81. R. I. Cooper and B. T. M. Willis, *Acta Crystallogr. A* **60**, 322 (2004).

82. F. Garrido, L. Nowicki, and L. Thome, *Phys. Rev. B* **74**, 184114/1 (2006).

83. H. Y. Geng, Y. Chen, Y. Kaneta, and M. Kinoshita, *Appl. Phys. Lett.* **93**, 201903 (2008).

84. L. Desgranges, G. Baldinozzi, G. Rousseau, J.-C. Niepce, and G. Calvarin, *Inorg. Chem.* **48**, 7585 (2009).

85. L. Desgranges, G. Badinozzi, D. Simeone, and H. E. Fischer, *Inorg. Chem.* **50**, 6146 (2011).

86. J. C. Crowhurst et al., *J. Phys.-Condens. Mat.* **27**, 265401 (2015).

87. H. M. He, A. D. Andersson, D. D. Allred, and K. D. Rector, *J. Phys. Chem. C* **117**, 16540 (2013).

88. P. Ruello, G. Petot-Ervas, and P. C., *J. Am. Ceram. Soc.* **88**, 604 (2005).

89. J. M. DeLeon, S. D. Conradson, T. Tyson, A. R. Bishop, M. Salkola, F. J. Espinosa, and J. L. Pena, in *Applications of Synchrotron Radiation Techniques to Materials Science III*, edited by L. J. Terminello, S. M. Mini, H. Ade and D. L. Perry (Cambridge University Press, 1996), Vol. 437, p. 189.

90. J.-Y. Li et al., in *ArXiv e-prints*, 2010), p. 1.

91. K. W. Kim, G. D. Gu, C. C. Homes, and T. W. Noh, *Phys. Rev. Lett.* **101**, 177404 (2008).

92. H. Okamoto, T. Miyagoe, K. Kobayashi, H. Uemura, H. Nishioka, H. Matsuzaki, A. Sawa, and Y. Tokura, *Phys. Rev. B* **83**, 125102 (2011).

93. L. Perfetti, P. A. Loukakos, M. Lisowski, U. Bovensiepen, H. Eisaki, and M. Wolf, *Phys. Rev. Lett.* **99**, 197001 (2007).

94. V. Brouet et al., *Phys. Rev. B* **87**, 041106(R) (2013).

95. M. Bauer, A. Marienfeld, and M. Aeschlimann, *Prog. Surf. Sci.* **90**, 319 (2015).

96. D. Wegkamp and J. Staehler, *Prog. Surf. Sci.* **90**, 464 (2015).

97. S. Gilbertson, G. L. Dakovski, T. Durakiewicz, J.-X. Zhu, K. M. Dani, A. D. Mohite, A. Dattelbaum, and G. Rodriguez, *J. Phys. Chem. Lett.* **3**, 64 (2012).

98. R. Yusupov, T. Mertelj, V. V. Kabanov, S. Brazovskii, P. Kusar, J. H. Chu, I. R. Fisher, and D. Mihailovic, *Nature Phys.* **6**, 681 (2010).

99. D. A. Andersson, J. Lezama, B. P. Uberuaga, C. Deo, and S. D. Conradson, *Phys. Rev. B* **79**, 024110 (2009).

100. D. A. Andersson, F. J. Espinosa-Faller, B. P. Uberuaga, and S. D. Conradson, *J. Chem. Phys.* **136**, 234702 (2012).

101. J. M. Deleon, S. D. Conradson, I. Batistic, and A. R. Bishop, *Phys. Rev. Lett.* **65**, 1675 (1990).

102. J. M. Deleon, S. D. Conradson, I. Batistic, A. R. Bishop, I. D. Raistrick, M. C. Aronson, and F. H. Garzon, *Phys. Rev. B* **45**, 2447 (1992).

103. J. M. Deleon, G. G. Li, and S. D. Conradson, *Physica C* **220**, 377 (1994).

104. I. B. Bersuker, *The Jahn-Teller Effect* (Cambridge University Press, New York, 2006).

105. R. Caciuffo, G. Amoretti, P. Santini, G. H. Lander, J. Kulda, and P. D. Du Plessis, *Phys. Rev. B* **59**, 13892 (1999).

106. S. D. Conradson, D. Manara, F. Wastin, D. L. Clark, G. H. Lander, L. A. Morales, J. Rebizant, and V. V. Rondinella, *Inorg. Chem.* **43**, 6922 (2004).

107. L. F. He, M. Gupta, M. A. Kirk, J. Pakarinen, J. Gan, and T. R. Allen, *JOM* **66**, 2553 (2014).

108. R. Mankowsky et al., *Nature* **516**, 71 (2014).

109. M. Mitrano et al., *Nature* **530**, 461 (2016).

110. A. Vittorini-Orgeas and A. Bianconi, *J. Supercond. Nov. Magn.* **22**, 215 (2009).

111. D. Nicoletti et al., *Phys. Rev. B* **90**, 100503 (2014).

112. C. A. Regal, M. Greiner, and D. S. Jin, *Phys. Rev. Lett.* **92**, 040403 (2004).

113. Y. I. Shin, C. H. Schunck, A. Schirotzek, and W. Ketterle, *Nature* **451**, 689 (2008).

114. J. A. Bradley et al., *J. Am. Chem. Soc.* **132**, 13914 (2010).

115. Y. Q. An, A. J. Taylor, S. D. Conradson, S. A. Trugman, T. Durakiewicz, and G. Rodriguez, *Phys. Rev. Lett.* **106**, 207402 (2011).

116. T. R. Griffiths, H. V. S. Hubbard, G. C. Allen, and P. A. Tempest, *J. Nucl. Mater.* **151**, 307 (1988).

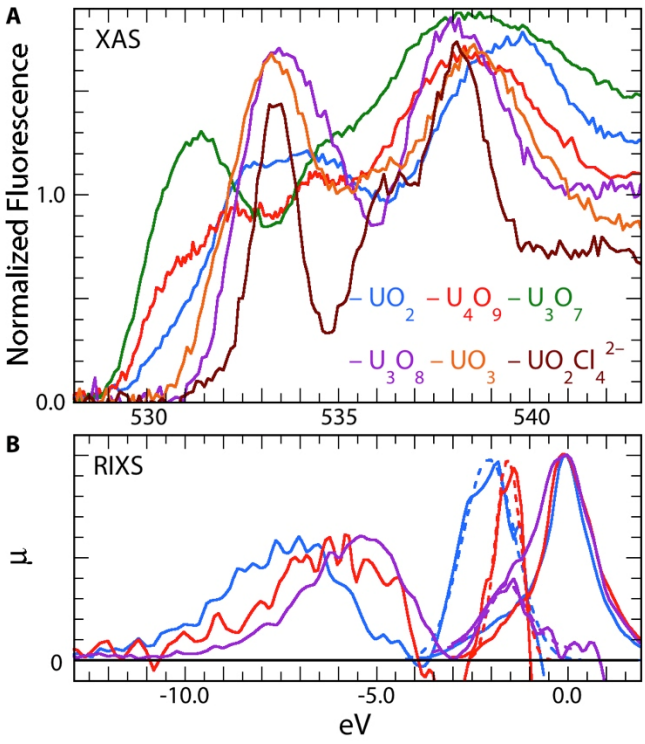

Figure 1. O XAS and U M RIXS of UO_{2+x} and standards. (A) The energies for the UO_2, U_4O_9, and U_3O_7 XAS were obtained from the NIXS measurements and the others adjusted from literature values[32] to this UO_2. The broadening of the overall 5*f*-6*d* manifold of the mixed valence compounds occurs on the low energy edge of the upper Hubbard band. In addition to some variability in the relative amplitudes between different samples of the same compound (Fig. S1), the NIXS that is not distorted by self-absorbance shows that the 531.5 eV peak in the U_3O_7 spectrum is quite low relative to the others (Fig. S3). **(B)** The U M_5 valence-to-core 3*d*5*f* RIXS, consisting of the U 5*f*→O 2*p* and intra-atomic U 5*f*→5*f* excitations at, respectively, energy transfers of <-3.5 eV and -4–0 eV, and the elastic peak at 0 eV. The original spectra from around -4 eV to 2 eV that contains the elastic peak at 0 eV that overlaps with the U 5*f* peak on its low energy side are plotted on a larger scale to facilitate inspection of the RIXS that are lower in amplitude. The spectra over this range were then curve-fit with two Voigt functions and the one for the elastic peak was subtracted from the spectra that are plotted over the entire range on a smaller scale so that they are magnified relative to the elastic peak. The O 2*p* states are therefore seen at <-3.5 eV and the U 5*f* states at -4–0 eV. The dashed lines are the curve-fits for the U 5*f* peak.

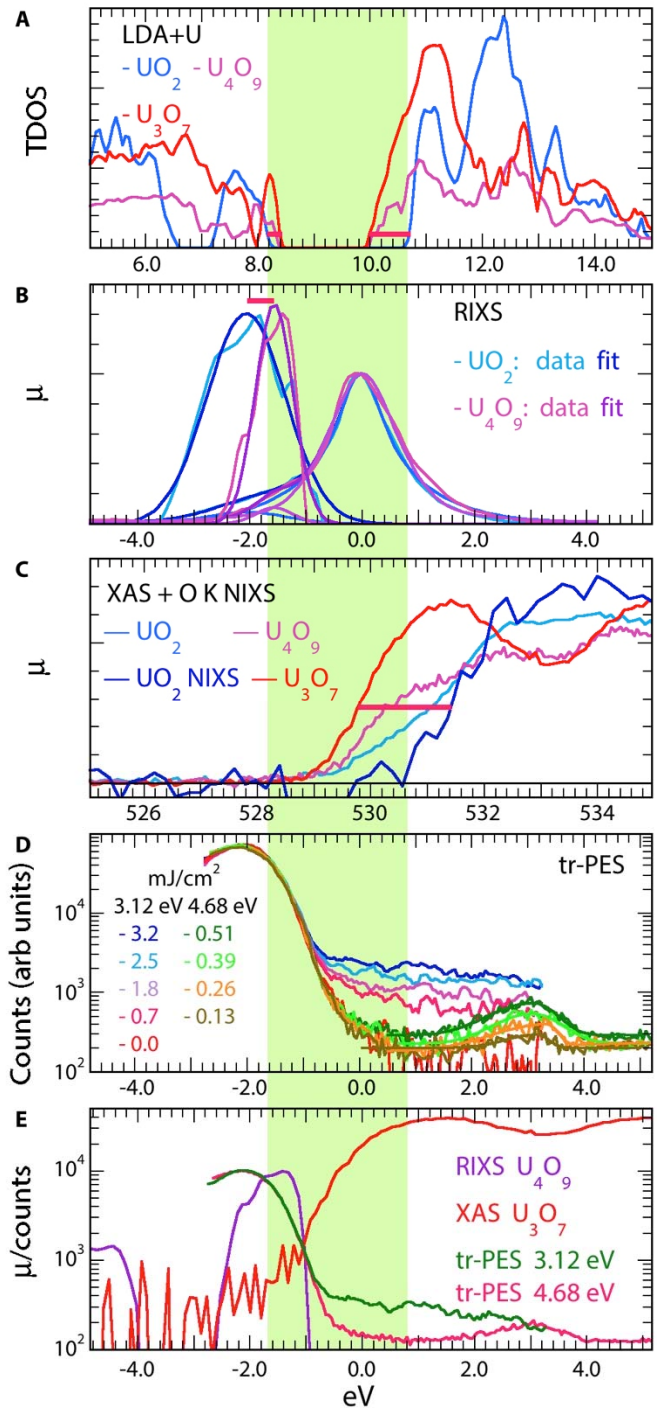

Fig. 2. Tracking the Mott gap in O- and Photo-doped $UO_{2(+x)}$. (A) LDA+U calculations of the total densities of states (DOS) for UO_2, U_4O_9, and U_3O_7 using the static, U(IV,V)-based structures derived from neutron scattering and energy minimization. **(B)** U M_5 RIXS of UO_2 and U_4O_9 showing the measured spectra that are the overlapping elastic and occupied U 5*f* peaks of the LHB scaled to a peak height of one, the fits to two Voigt functions, the individual components of the fits, and the separated U 5*f* contributions to the data and their fits. **(C)** O XAS of UO_2, U_4O_9, and U_3O_7 showing the transitions to the unoccupied states of the UHB of predominantly U 5*f* character. The NIXS of UO_2 does not show the low energy tail displayed by the more surface sensitive XAS measurement. **(D)** 40 fs resolution pump-probe angle-integrated photoemission measurements coincident with the excitation pulse excited at the listed fluences

with 3.1 and 4.7 eV pump energies. The solid lines at 0-5 eV are fits of the data to asymmetric Gaussian functions. The vertical green band is the 2.4 eV wide band gap, aligned with the calculation. The magenta bars show the shifts of the U_4O_9/U_3O_7 band edges or centroid relative to UO_2. The RIXS and tr-PES spectra with their different energy scales are aligned with respect to the center of the UO_2 5*f* states, with "0" energy = the elastic scattering for the RIXS and the Fermi level for the PES. The absorption edge of the UO_2 NIXS is aligned with the front portion of the DOS from the calculations and may exaggerate the actual width of the Mott gap. **(E)** Combined U_4O_9 RIXS after subtraction of the elastic peak, U_3O_7 XAS, and tr-PES at the highest fluence of both 3.1 and 4.7 eV excitation. Energy scales are the same as in the prior figures. The DOS from all of the measurements overlap around -1.0 eV with a nodal point a few percent of the maximum values, after adjusting the baselines to zero and scaling the maximum amplitudes of the RIXS and PES to 10,000 and the XAS to 30,000 to correspond to the calculation.

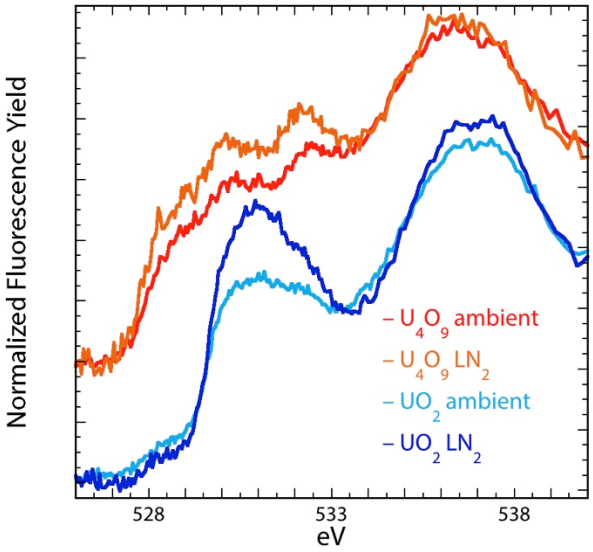

Fig. 3. O XAS of UO_2 and U_4O_9 at ambient and liquid N_2 temperature. The changes in the spectra on cooling that are much larger in the region dominated by the 5*f* states are indicative of a redistribution of the mobile charges that, for UO_2, should be more on the surface because bulk structure measurements show no temperature dependence, in contrast to EPR of powders.

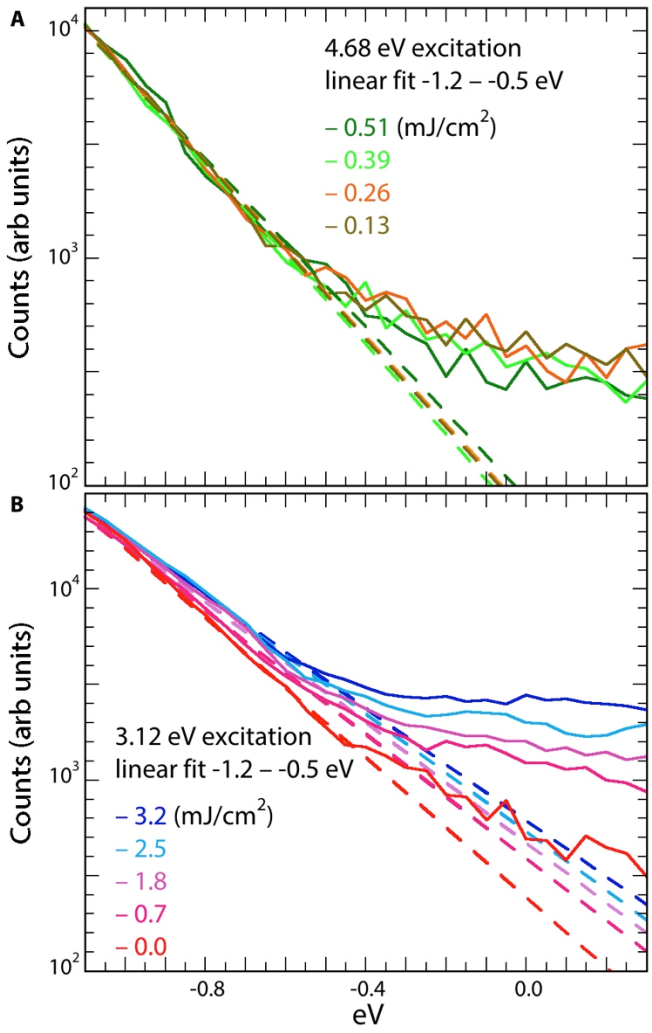

Fig. 4. **Fluence dependence on temperature at t=0.** Linear fits to the logarithm of the intensity over the leading edge of the photoemission peak nearest the Fermi level are indicative of the temperature of the thermalized hot electrons after the photon impulse. Because UO_2 is an insulator the linear portion of the ln(DOS) provides qualitative information rather than a specific temperature. **(A)** 4.7 eV excitation does not have a thermalized component, suggesting that it is totally relaxed within the 40 fs time resolution. **(B)** The monotonic increase in the x intercept with increasing fluence shows that the energy from 3.1 eV excitation relaxes sufficiently quickly within the same time interval to give this thermalized component whose temperature increases with increasing energy.

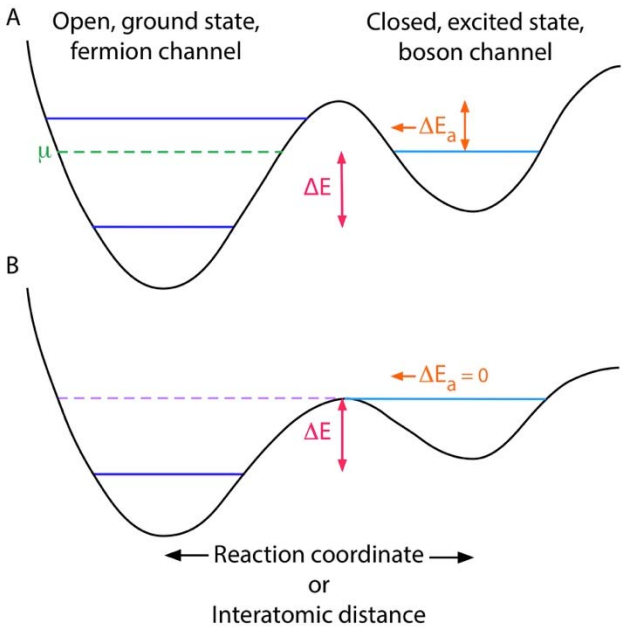

Fig. 5. **Potentials/reaction coordinates for asymmetric double well potentials for fermion pairing.** The pair potential is the curve across its entire range, the reaction coordinate is the range between the arrows. **(A)** Athough energetically favored by ΔE, relaxation of the excited state is inhibited by an activation energy with a barrier height of E_a, promoting the accumulation of particles to give an excess, non-equlibrium population in the closed channel that will become the condensate. The inhibition is maximized when the energy of the excited state is in proximity to the chemical potential that will be between the occupied ground state and lowest unoccupied state. **(B)** Coherent transfer between the open and closed channels is promoted by a Fano-Feshbach resonance that is maximized when the energy of the excited, S=0 state is in proximity to the invididual particle energy of the S≠0 state. The barrier height for the reverse reaction is therefore zero. ΔE for UO_{2+x} = -2.2 eV, which is very close to the energy between the centers of the U_4O_9 U 5*f* highest occupied state and the and the lowest feature in the UO_{2+x} spectra (Figs. 2B and C) that corresponds to the lowest energy excited state.